

Analysis Congo red dye adsorption on hydrochar and nano-hydrochar from *Areca catechu*: Synthesis, characterization, and comparative study

Robiatul Adawiyah¹, Yulizah Hanifah², Neza Rahayu Palapa^{3*}

¹ Master of Materials Science, Graduate Program, Sriwijaya University, Palembang, 30139, Indonesia

² National Research and Innovation Agency, PUSPIPTEK, Tangerang Selatan, 15311, Indonesia

³ Department of Chemistry, Faculty of Mathematics and Natural Sciences, Sriwijaya University, Palembang, 30662, Indonesia

* Corresponding author's e-mail: nezarahayu@mipa.unsri.ac.id

ABSTRACT

Industrial wastewater containing dyes like Congo red poses serious environmental and health risks due to its high toxicity, resistance to conventional treatments, and stability under environmental conditions. Adsorption has emerged as a promising alternative for dye removal due to its simplicity, cost-effectiveness, and sustainability. In this study, hydrochar (HC) and nano-hydrochar (nano-HC) were synthesized from *Areca catechu* (betel nut husk) and evaluated for their ability to adsorb Congo red. High-energy milling was applied to reduce the hydrochar to nanoscale, significantly enhancing its surface area, active site availability, and adsorption efficiency. Nano-HC demonstrated a maximum adsorption capacity of 596.617 mg/g, surpassing HC (356.132 mg/g) and raw *Areca* husk (128.654 mg/g). The adsorption process followed pseudo-second-order kinetics and Langmuir isotherm models, indicating chemisorption and monolayer adsorption behavior. The findings highlight the potential of *Areca catechu*-derived nano-HC as an eco-friendly, cost-effective adsorbent for dye-contaminated wastewater treatment. This study emphasizes the importance of sustainable biomass utilization and advances in particle engineering for environmental remediation.

Keywords: *Areca catechu*, Congo red adsorption, hydrochar, nano-hydrochar, and dye removal.

INTRODUCTION

Industrial wastewater is a significant environmental and public health challenge, particularly due to the widespread use of synthetic dyes across various industries. Sectors such as textiles, plastics, paper, and leather manufacturing are the primary contributors to dye pollution (Hammud et al., 2023). These industries generate significant amounts of effluents containing hazardous chemical compounds, which are often discharged untreated or inadequately treated into natural water bodies (Emmanuel and Adesibikan, 2024a). The presence of dyes in wastewater is a major concern. They are highly stable, resistant to biodegradation, and toxic to aquatic ecosystems and human health. Congo red (CR),

a widely utilized anionic diazo dye, is of special concern among the dyes commonly found in industrial effluents due to its persistence and toxicity (Harja et al., 2022). It is used extensively in the textile and pigment industries because it provides vibrant color and stability under varying pH and temperature conditions (Li et al., 2016). However, its durability also contributes to environmental pollution. It resists breakdown in conventional wastewater treatment processes such as aerobic and anaerobic digestion. Congo red metabolizes into benzidine, a well-documented carcinogen that poses severe risks to human and ecological health. Furthermore, Congo red's strong resistance to light, heat, and moderate oxidants makes it extremely difficult to remove from wastewater, leading to its accumulation in

aquatic environments (Hua et al., 2023). This highlights the critical need for innovative, effective, and sustainable methods for dye removal.

Over the past decades, numerous technologies have been developed to treat dye-contaminated wastewater. These range from physical methods such as coagulation and filtration to advanced chemical and biological treatments (Siregar et al., 2021). However, these methods are often associated with significant drawbacks, including high operational costs, the generation of secondary pollutants, and the requirement for sophisticated technical expertise (Khan et al., 2023). Chemical oxidation is an effective method for dye degradation, but it often produces harmful byproducts. Similarly, membrane filtration is effective but expensive and prone to fouling, which limits its large-scale applicability (Goyi et al., 2024). It is imperative that we explore alternative treatment methods that are both cost-effective and environmentally sustainable.

Adsorption is the method of choice for removing dyes from wastewater. It is simple to operate, low-cost, and has minimal environmental impact (Zhou et al., 2024). Adsorption is a process that involves the physical or chemical interaction between dye molecules (adsorbates) and a solid material (adsorbent), which captures and removes contaminants from wastewater (Gao et al., 2016). The performance of adsorption processes is influenced by several factors, including the surface area, porosity, and functional groups of the adsorbent material (Jalilian et al., 2024a). Furthermore, adsorption is the optimal solution due to its high efficiency, adaptability for a wide range of contaminants, and minimal production of secondary waste.

In recent years, a variety of adsorbent materials have been developed, including activated carbon (Tabassum et al., 2020), carbon nanotubes (CNTs) (Ren et al., 2011), graphene (Wang et al., 2015), biochar (Sharma et al., 2022), hydrochar (Li et al., 2016), and composite materials (Wijaya et al., 2021). Hydrochar is a carbon-rich material produced through hydrothermal carbonization of biomass is the one to watch. Hydrochar is the optimal choice for wastewater treatment due to its unique properties, including a high carbon content, tunable surface characteristics, and ease of production (Hasanah et al., 2022). Recent studies have demonstrated the potential of hydrochar derived from various biomass sources for dye adsorption, with varying adsorption capacities

(Q_{max}) depending on the feedstock and synthesis conditions. For instance, hydrochar from bamboo sawdust showed a Q_{max} of 33.7 mg/g for CR (Li et al., 2016), while rice straw-derived hydrochar exhibited a Q_{max} of 222.1 mg/g for CR (Li et al., 2019). However, there remains a gap in the development of hydrochar-based materials with significantly enhanced adsorption capacities, particularly through nanoscale modifications.

The novelty of this research lies in the synthesis of nano-hydrochar from *Areca catechu* husk biomass using a simple yet highly effective high-energy milling (HEM) method (Rojas-Chávez et al., 2020). This approach transforms conventional hydrochar into nano-hydrochar, significantly enhancing its adsorption capabilities while maintaining a cost-effective and scalable production process. The HEM method not only reduces particle size to the nanoscale but also increases the material's surface area, porosity, and availability of active sites, which are critical for efficient dye adsorption (Zhang et al., 2004).

The reduction of particle size to the nanoscale is undoubtedly one of the most significant advancements in adsorbent development (Chausali et al., 2021). This process dramatically enhances the material's adsorption properties. High-energy milling is an effective method for transforming hydrochar into nano-hydrochar, resulting in smaller particles with higher surface areas and more active adsorption sites (Kumar et al., 2020). Nano-hydrochar exhibits superior adsorption kinetics, due to improved dye-adsorbent interactions, higher porosity, and better dispersibility in aqueous solutions (Zhang et al., 2004). Nano-hydrochar is the ideal solution for removing complex dyes like Congo red.

Areca catechu, commonly known as betel nut husk, is a highly sustainable and abundant biomass source that can be used for adsorbent development. It is widely available as agricultural waste in tropical regions and is an ideal precursor for producing hydrochar and nano-hydrochar due to its high carbon content (Chao et al., 2020). Using *Areca catechu* husk is the best way to create a low-cost material for adsorbent synthesis while also promoting the valorization of agricultural waste. This aligns perfectly with the principles of the circular economy and sustainable development.

This study synthesizes and characterizes hydrochar and nano-hydrochar derived from *Areca catechu* husk for the adsorption of Congo red dye

from wastewater. This research will compare the physicochemical properties of raw Areca husk, hydrochar, and nano-hydrochar. We will evaluate the adsorption performance of these materials based on key parameters, including adsorption capacity, kinetics, and isotherm behavior. We will also investigate the role of high-energy milling in enhancing the adsorption efficiency of hydrochar. The findings of this study will contribute to the development of eco-friendly, efficient, and scalable adsorbents for industrial wastewater treatment. This will address the global challenge of dye pollution while promoting the sustainable utilization of agricultural waste.

EXPERIMENTAL SECTION

Chemicals and instrumentation

Materials used in this research include distilled water (H₂O) from PT. Dira Sonita, HCl, NaOH, NaCl, Congo red dye (C₃₂H₂₂N₆Na₂O₆S₂), and *Areca catechu* L. sourced from Pangandaran, West Java, Indonesia. Equipment utilized includes measuring cups, beakers, vacuum, hot-plate, funnel, filter paper, analytical balance, oven, magnetic stirrer, pH meter, thermometer, pipettes, centrifuge, hydrothermal stainless-steel autoclave, XRD Rigaku Miniflex-6000, Quantachrome Micrometric ASAP and UV-Vis Biobase BK-UV 1800 PC spectrophotometer.

Preparation of hydrochar from *Areca catechu* husk

The preparation of hydrochar began by weighing 2.5 grams of Areca husk, which was then mixed with 50 mL of distilled water in a 100 mL stainless-steel hydrothermal autoclave. The autoclave was sealed tightly and placed in an oven preheated to 250 °C, where it was maintained for 4 hours to undergo the hydrothermal carbonization process. Once the reaction was complete, the autoclave was allowed to cool naturally to room temperature (Pauletto et al., 2021).

The solid product, referred to as hydrochar, was collected from the autoclave and washed thoroughly with distilled water multiple times to remove any residual impurities, such as soluble organic and inorganic compounds. After washing, the hydrochar was dried in a conventional oven

set to 105 °C for 24 hours to ensure complete removal of moisture.

Preparation of nano-hydrochar from *Areca catechu* husk

To convert the hydrochar into nano-hydrochar, the hydrochar that have been prepared before was subjected to particle size reduction using high-energy milling (HEM). Approximately 2.5 grams of the dried hydrochar was placed into the milling chamber of a HEM device, equipped with stainless steel balls as the grinding medium. The milling process was conducted at a rotational speed of 500 rpm for 3 hours, with periodic pauses every 30 minutes to prevent overheating and ensure uniform grinding. After milling, the resulting nano-hydrochar was sieved using a fine mesh (200 mesh) to separate uniform-sized nanoparticles from any larger agglomerates (Rojas-Chávez et al., 2020). The obtained nano-hydrochar powder was then stored in an airtight container to prevent contamination and moisture absorption. Nano-hydrochar was characterized using techniques such as scanning electron microscopy (SEM) to analyze its morphology, fourier transform infrared spectroscopy (FTIR) to identify functional groups, Brunauer-Emmett-Teller (BET) analysis to measure surface area and porosity, and x-ray diffraction (XRD) to confirm its crystalline structure. These characterizations ensure that the nano-hydrochar meets the desired properties for adsorption applications.

Adsorption study

Each solution is adjusted to a pH range of 2–11 using 0.1 M NaOH or 0.1 M HCl. After the pH adjustment, 0.02 g of hydrochar, nano-hydrochar derived from Areca husk is added to the solution. The mixture is then agitated on a shaker for 24 hours. Following this process, the filtrate is collected, and the final pH is measured using a pH meter. Each treatment is performed in triplicate to ensure accuracy and reproducibility.

Several parameters, such as concentration, pH, and temperature, were tested to identify the ideal conditions for the dye adsorption process. In the pH variation experiment, a 20 mL dye solution with a concentration of 50 mg/L was prepared, and the pH was adjusted between 3 and 11 using NaOH and HCl solutions. After pH adjustment, the initial absorbance was measured using

a UV-Vis spectrophotometer to assess how pH affected the adsorption performance. For the adsorption experiment, 0.02 g of Areca husk adsorbent hydrochar and nano-hydrochar were added to a 100 mL Erlenmeyer flask containing 20 mL of dye solution at a concentration of 50 mg/L, without altering the pH of the dye. The mixture was stirred using a magnetic stirrer at intervals of 10, 20, 30, 40, 50, 60, 90, 120, 150, and 180 minutes. After each stirring period, the adsorbent and remaining dye were separated by filtration, and the filtrate was collected. The absorbance of the filtrate was then measured using a UV-Vis spectrophotometer. At each interval, the suspension was filtered to separate the solid adsorbent from the remaining dye solution. The resulting filtrate was analyzed using a UV-Vis spectrophotometer to measure its absorbance, providing data on the dye concentration left in the solution. This procedure was repeated under controlled conditions to assess adsorption efficiency based on stirring time and the type of adsorbent used (Normah et al., 2021).

The effect of dye concentration was explored by preparing solutions with varying concentrations between 50, 100, 150 and 200 mg/L. For each concentration, 0.02 g of adsorbent was added, stirred for two hours, and filtered. The filtrate was then analyzed with a UV-Vis spectrophotometer to quantify the remaining dye concentration. The impact of temperature was examined by conducting the experiment at controlled temperatures of 30 °C, 40 °C, 50 °C, and 60 °C while following the same stirring and separation protocols (Dai et al., 2019).

Additionally, the reusability of the adsorbents was evaluated by performing regeneration and desorption tests. Used adsorbents were introduced into a 20 mL solution containing 50 mg/L of dye and stirred for two hours. Afterward, the remaining dye concentration in the solution was measured using a UV-Vis spectrophotometer. The adsorbents were then subjected to desorption through ultrasonic treatment in 25 mL of aqueous solvent for two hours, followed by filtration. The recovered adsorbents were dried and reused in subsequent experiments to assess their regeneration capabilities (Palapa et al., 2021).

RESULT AND DISCUSSION

The XRD diffractogram in Figure 1 shows the structural characteristics of Areca husk, hydrochar (HC), and nano-hydrochar (nano-HC). The Areca husk exhibits peaks at 16.58° and 22.25°, along with smaller peaks at 53.74° and 60.08°, indicating semi-crystalline properties with a significant amorphous fraction due to the presence of cellulose and hemicellulose. For HC, peaks at 15.88°, 22.92°, and 34.74° suggest an increase in structural organization after hydrothermal carbonization, with the prominent peak at 22.92° indicating partially ordered carbon, though the structure remains largely amorphous (Bardalai and Mahanta, 2018). In contrast, nano-HC displays a broad peak at 22.25° with reduced intensity, reflecting a highly disordered and amorphous

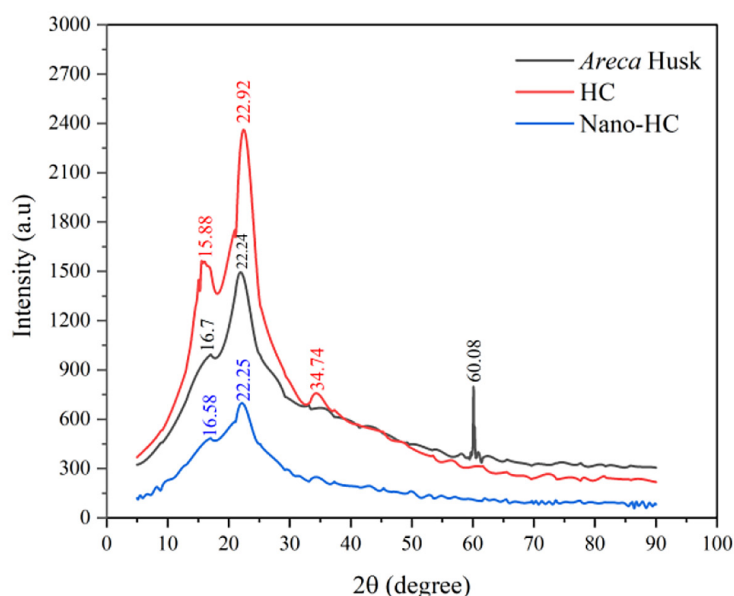


Figure 1. X-ray diffraction of Areca husk, HC and nano HC

structure caused by high-energy milling, which enhances surface area and adsorption capability. These results demonstrate a transition from semi-crystalline to more amorphous structures, aligning with studies showing that thermal treatment and particle size reduction improve adsorbent performance by increasing active surface sites (Mahmoud et al., 2024).

The FTIR spectrum presented in Figure 2 illustrates the functional group compositions of Areca husk, HC, and nano-HC. The Areca husk exhibits a broad absorption band at 3400–3200 cm^{-1} , indicative of O–H stretching vibrations from hydroxyl groups, suggesting the presence of moisture or hydrogen-bonded alcohols and phenols. Peaks around 2920 cm^{-1} and 2850 cm^{-1} correspond to asymmetric and symmetric C–H stretching in aliphatic chains, indicating fatty acid or cellulose components (Singh and Garg, 2024). In HC, peaks at 1650–1600 cm^{-1} represent C=C stretching vibrations from aromatic rings, reflecting increased aromaticity during hydrothermal carbonization (Emmanuel and Adesibikan, 2024b). Additionally, the band at 1400 cm^{-1} corresponds to C–H bending vibrations, while the peak at 1110 cm^{-1} suggests C–O–C stretching, characteristic of ether linkages in carbohydrate residues. Nano-HC demonstrates a notable reduction in peak intensity, particularly at 1110 cm^{-1} and 1600 cm^{-1} , implying structural modifications from high-energy milling that disrupt aromatic and ether groups, enhancing surface functionalization (Bo and Shi, 2024). The peaks at 600–800

cm^{-1} indicate the presence of aromatic out-of-plane bending, confirming the retention of aromatic structures in the adsorbent materials. These spectra reveal that the surface chemistry of HC and nano-HC is enriched with functional groups such as hydroxyl, carbonyl, and aromatic groups, improving their adsorption capabilities for dye removal (Guo et al., 2015).

The SEM images of *Areca catechu* fruit husk, biochar, and nano-biochar reveal distinct surface morphologies. Figures 3a and 3b depict small spherical fragments with visible micropores on the *Areca catechu* husk surface. However, the porosity is less pronounced compared to the biochar shown in Figures 3c and 3d, where the hydrothermal carbonization process widens the pores due to the decomposition of organic matter. In Figures 3e and 3f, the nano-biochar exhibits smaller particle sizes but shows signs of agglomeration caused by strong interparticle forces at the nanoscale. Nano-hydrochar were milled using High-Energy Milling at 500 rpm for 3 hours, resulting in a material with a tubular, elongated structure and fine particle size (Vinayagam et al., 2023).

The raw Areca husk displays a rough and uneven surface with large aggregates and cracks, reflecting its natural fibrous texture. These characteristics suggest limited adsorption performance due to irregular pore distribution and reduced surface area. In contrast, the hydrochar exhibits a more compact and uniform structure with visible micro-porous regions, though the pores are not yet fully developed (Jalilian et al., 2024b).

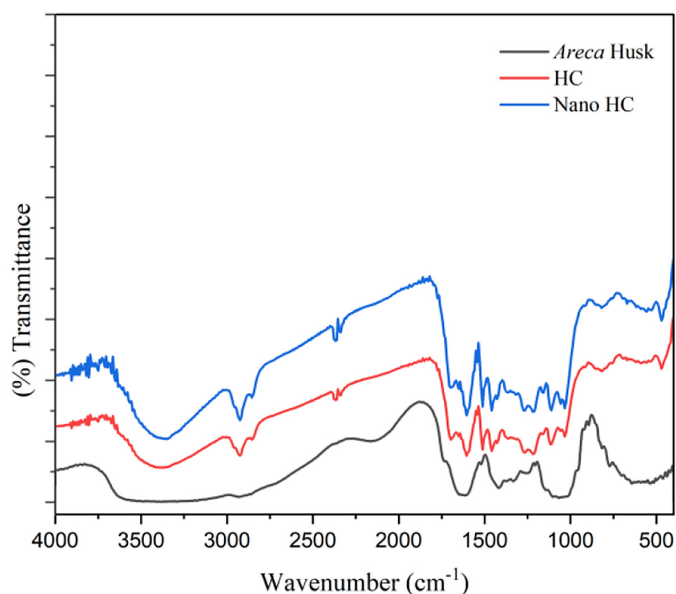


Figure 2. FTIR spectra of Areca husk, HC and nano HC

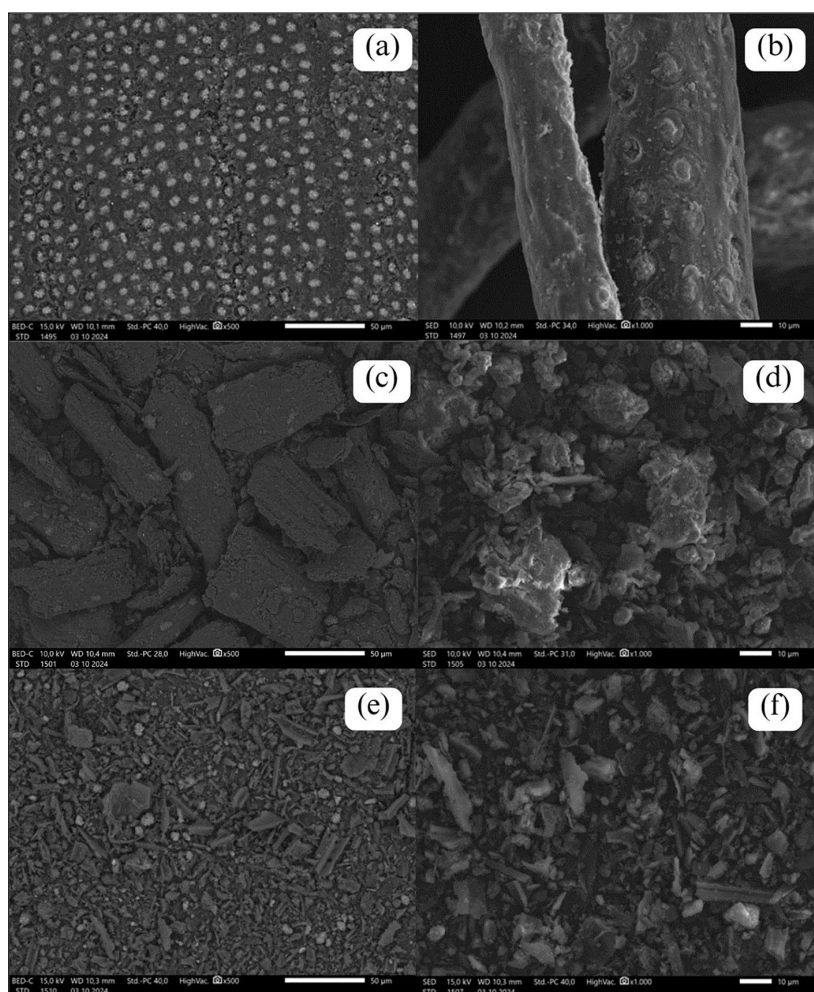


Figure 3. SEM image of Areca husk x500 (a), Areca husk x1000 (b), HC x500 (c), HC x1000 (d), nano HC x500 (e) and nano HC x1000 (f)

This indicates that the hydrothermal process partially enhances the material's surface properties, improving its adsorption potential compared to the raw husk. The nano-hydrochar, however, shows a highly fragmented structure with finer particle distribution and significantly increased porosity (Haris et al., 2022). The well-defined and smaller pores contribute to a higher specific surface area, enhancing its adsorption capability. These morphological transformations align with the experimental results, where nano-hydrochar demonstrates superior adsorption performance, as indicated by its higher Langmuir adsorption capacity (Q_{max}).

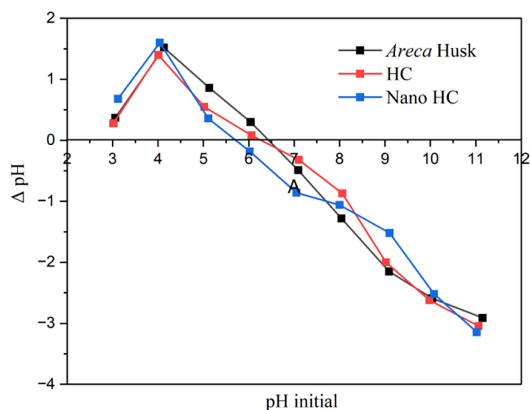
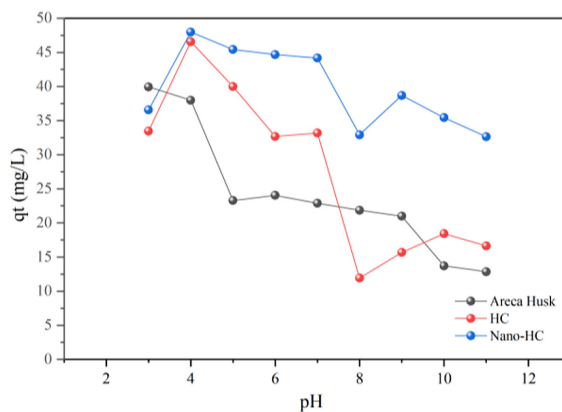
The EDX results on Table 1. show a significant increase in carbon content, from 51.13% in Areca husk to 59.18% in hydrochar and 75.36% in nano-hydrochar, with a corresponding decrease in oxygen content, indicating effective carbonization during processing. The decrease in oxygen (from 41.10% to 23.67% in % mass)

reflects the removal of oxygen-containing groups through hydrothermal and milling processes, enhancing the material's hydrophobicity and adsorption potential. Minimal changes in aluminum (Al) and silicon (Si) suggest these elements remain as trace impurities, unaffected by the treatment. These compositional improvements highlight nano-HC as a highly carbon-rich material with optimized properties for adsorption applications (Lin et al., 2023).

The pH point of zero charge (pH_{pzc}) values of Areca husk, hydrochar, and nano-hydrochar, as shown in the Figure 4, were determined to be approximately 6.05, 6.08, and 6.65, respectively. The pH_{pzc} represents the pH at which the net surface charge of the material becomes neutral. At pH values below the pH_{pzc} , the surface is positively charged, favoring the adsorption of anionic dyes like Congo red due to electrostatic attraction. Conversely, at pH values above the pH_{pzc} , the surface becomes negatively charged, repelling

Table 1. EDX result of Areca husk, HC and nano-HC

Adsorbent	Element % mass				Element % atom			
	C	O	Al	Si	C	O	Al	Si
Areca husk	51.13%	41.10%	0.90%	6.87%	59.92%	36.16%	0.47%	3.44%
HC	59.18%	39.82%	0.35%	0.65%	66.12%	33.40%	0.17%	0.31%
Nano HC	75.36%	23.67%	0.31%	0.66%	80.56%	18.99%	0.15%	0.30%

**Figure 4.** pHpzc point zero charge of Areca husk, HC and nano HC**Figure 5.** Impact of pH adsorption to Areca husk, hydrochar and nano-hydrochar

anionic molecules and reducing adsorption efficiency. The nano-HC shows a slightly higher pHpzc compared to HC and Areca husk, indicating its improved surface modification through high-energy milling, which likely enhances its adsorption capacity at near-neutral pH conditions (Waly et al., 2024).

In this study, the adsorption process was conducted at the natural pH of Congo red (6.16) without adjusting the solution's pH. This decision was made to better simulate real-world applications and to avoid altering the structural integrity of the adsorbents. At pH 6.16, the surface charges of HC and nano-HC are near their pHpzc, allowing for sufficient electrostatic attraction to Congo red molecules while maintaining material stability (Liu et al., 2024). Avoiding pH modification also ensures that the adsorption performance observed reflects the inherent properties of the materials, thus providing a more environmentally compatible approach to wastewater treatment using these adsorbents (Supraja et al., 2023).

Figure 5 describe that amount of Congo red absorbed by Areca husk, hydrochar and nano-hydrochar depends heavily on the pH. Acidic pH levels ranging from 2 to 4 protonate all adsorbent surfaces, considerably improving adsorption via strong electrostatic attraction to the anionic dye.

nano-hydrochar's adsorption capacity, like that of other materials, peaks at pH 5–6; however, this is especially pronounced for nano-hydrochar due to its larger surface area and greater number of active sites. Outside this precise range, the adsorbent's efficiency decreases considerably because its strongly negative surface charge causes large electrostatic repulsion and competes heavily with many hydroxide ions at alkaline pH.

Areca husk, HC and nano-HC have pH points of zero charge (pHpzc) values near 6.05, 6.08 and 6.65. Below these pH values, they are positively charged, improving adsorption through electrostatic interactions. Near-neutral pH conditions of 6.16 proved sufficient for all adsorption experiments; electrostatic attraction alone was adequate, eliminating the need for pH adjustment. Adsorption is also influenced by hydrogen bonding, π - π interactions and other interactions. Nano-HC shows outstanding potential for wastewater treatment, especially when operating near its pHpzc to improve electrostatic interactions.

The adsorption kinetics on Table 2 and Figure 6 shows Congo red adsorption onto Areca husk, HC, and nano HC were analyzed using pseudo-first-order (PFO) and pseudo-second-order (PSO) models to understand the adsorption mechanism. The parameters for each model were

Table 2. Kinetics adsorption result

Adsorbent	Initial concentration	Qe exp (mg/g)	PFO			PSO		
	(mg/L)		Qe calc (mg/g)	R ²	k ₁	Qe calc (mg/g)	R ²	k ₂
Areca husk	50.74	36.348	15.129	0.784	-5.711	36.731	0.995	0.002
HC	50.74	38.263	12.497	0.657	-5.156	38.239	0.995	0.003
Nano HC	51.82	40.644	9.523	0.661	-7.546	48.487	0.999	0.007

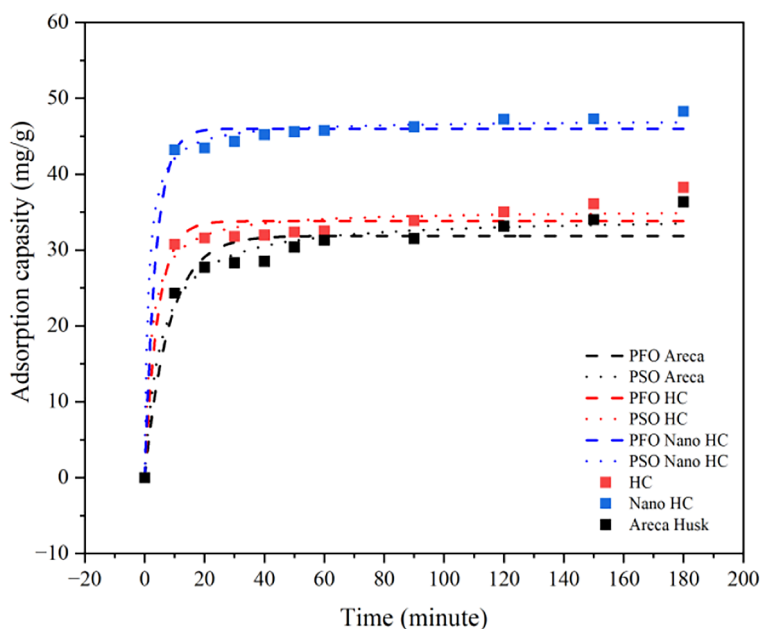


Figure 6. Adsorption kinetics pseudo-first order kinetic model and pseudo-second order kinetic model of Areca husk, HC and nano HC

presented in Table 5. The equilibrium adsorption capacity (q_e) for Areca husk, HC, and nano HC was 36.348 mg/g, 38.263 mg/g, and 40.644 mg/g, respectively, indicating that nano HC exhibited the highest adsorption capacity due to its enhanced surface area and functional group density (Wang et al., 2022). The data showed that the PSO model provided a better fit for all adsorbents, with R^2 values of 0.995 for Areca husk and HC, and 0.999 for nano HC, compared to the lower R^2 values obtained using the PFO model. This suggests that the adsorption process is chemisorption-driven, controlled by electron sharing or exchange between CR and the adsorbent surfaces (Pauletto et al., 2021).

Figure 7 Shows the adsorption isotherms of Congo red were analyzed using Langmuir, Freundlich, and Temkin models to understand the nature and mechanisms of the adsorption process. The Langmuir isotherm, which assumes monolayer adsorption on a homogeneous surface, provided an excellent fit for Areca husk with an R^2

value of 0.999 and a maximum adsorption capacity (Q_{max}) of 123.748 mg/g at 30 °C. Hydrochar exhibited a higher Q_{max} of 224.589 mg/g but with a slightly lower R^2 of 0.903, indicating less uniform adsorption compared to Areca husk. Nano-hydrochar displayed the highest Q_{max} of 596.617 mg/g, reflecting its superior adsorption potential due to its enhanced surface area and nano-scale properties. The Langmuir model’s dominance for nano-HC and Areca husk suggests that monolayer adsorption, facilitated by functional groups such as -OH and -COOH, is the primary mechanism. This is further supported by the high R^2 values, indicating the availability of abundant uniform active sites on these adsorbents.

The Freundlich isotherm, which assumes a heterogeneous adsorbent surface with multilayer adsorption, showed a better fit for HC with an R^2 of 0.985, compared to 0.917 for Areca husk and 0.731 for nano-HC. The Freundlich constant (n), which indicates adsorption favorability, was highest for Areca husk (2.831), suggesting favorable

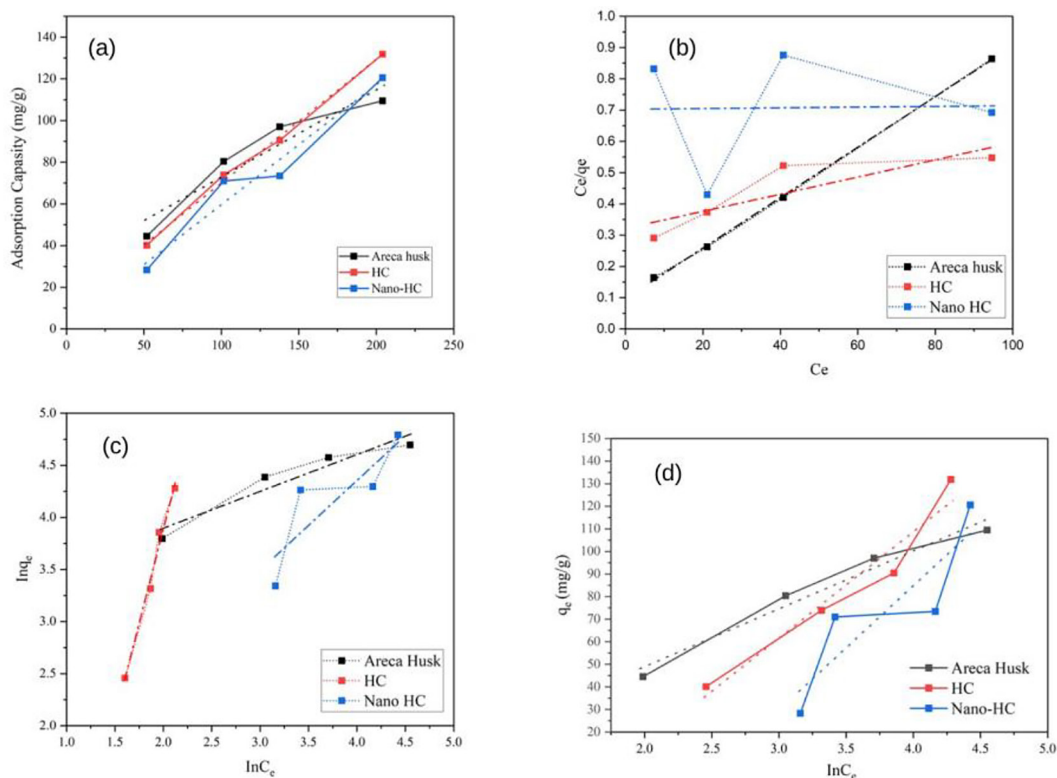


Figure 7. Concentration and adsorption capacity plots of Congo red adsorption (a) Langmuir isotherm, (b) Freundlich isotherm (c) and Temkin isotherm

adsorption, while HC and nano-HC had lower values of 1.592 and 1.161, respectively. The KF values further supported this trend, with Areca husk demonstrating the highest value (24.272), followed by HC (8.685) and nano-HC (2.479). These results indicate that while nano-HC has the highest adsorption capacity, its adsorption process is less influenced by the heterogeneity of the adsorbent surface compared to HC and Areca husk. This suggests that HC may involve contributions from multilayer adsorption and surface heterogeneity, as indicated by the relatively higher fit of the Freundlich model.

The Temkin isotherm, which considers the effects of adsorbent-adsorbate interactions and the heat of adsorption, also provided insights into the adsorption process. For Areca husk, the Temkin model showed a good fit with an R^2 of 0.966, indicating significant adsorbent-adsorbate interactions. HC and nano-HC also demonstrated reasonable fits with R^2 values of 0.946 and 0.764, respectively. The KT values, which represent the equilibrium binding constant, were highest for Areca husk (0.914), followed by HC (0.184) and nano-HC (0.085). The BT values, related to the heat of adsorption, were highest for nano-HC (54.937), suggesting stronger interactions at

higher temperatures. These findings highlight the complex nature of the adsorption process, with different isotherms providing complementary insights. Overall, the results demonstrate the potential of nano-HC as a highly effective adsorbent for CR removal, particularly in scenarios requiring high adsorption capacity, while Areca husk and HC offer alternative pathways with moderate capacity and diverse adsorption mechanisms.

Table 3. The adsorption isotherms of Congo red were analyzed using Langmuir, Freundlich, and Temkin models to understand the nature and mechanisms of the adsorption process. The Langmuir isotherm, which assumes monolayer adsorption on a homogeneous surface, provided an excellent fit for Areca husk with an R^2 value of 0.999 and a maximum adsorption capacity (Q_{max}) of 123.748 mg/g at 30°C. Hydrochar exhibited a higher Q_{max} of 224.589 mg/g but with a slightly lower R^2 of 0.903, indicating less uniform adsorption compared to Areca husk (Zahara et al., 2023). Nano-hydrochar displayed the highest Q_{max} of 596.617 mg/g, reflecting its superior adsorption potential due to its enhanced surface area and nano-scale properties. The Langmuir model's dominance for nano-HC and Areca husk suggests that monolayer adsorption, facilitated by

Table 3. Isotherm adsorption

Adsorbent	Adsorption isotherm	Adsorption constant	T			
			30 °C	40 °C	50 °C	60 °C
Areca husk	Langmuir	Q_{max}	123.748	112.361	87.746	68.493
		k_L	0.083	0.091	0.063	0.092
		R^2	0.999	0.853	0.791	0.933
	Freundlich	k_F	24.272	13.271	21.312	14.529
		R^2	0.917	0.913	0.917	0.936
		n	2.831	1.281	1.465	1.821
	Temkin	R^2	0.966	0.876	0.925	0.859
		K_T	0.914	0.812	0.941	0.965
		B_T	25.616	30.254	27.093	23.986
HC	Langmuir	Q_{max}	224.589	286.413	138.847	112.370
		k_L	0.017	0.046	0.015	0.027
		R^2	0.903	0.956	0.996	0.911
	Freundlich	k_F	8.685	2.931	4.142	8.639
		R^2	0.985	0.983	0.881	0.671
		n	1.592	1.252	1.606	1.855
	Temkin	R^2	0.946	0.876	0.918	0.953
		K_T	0.184	0.231	0.216	0.152
		B_T	47.066	50.218	45.195	48.982
Nano-HC	Langmuir	Q_{max}	596.617	595.750	497.151	388.239
		k_L	0.003	0.030	0.036	0.061
		R^2	0.056	0.875	0.871	0.944
	Freundlich	k_F	2.479	1.002	7.127	3.257
		R^2	0.731	0.742	0.744	0.668
		n	1.161	1.266	1.875	1.918
	Temkin	R^2	0.764	0.873	0.812	0.752
		K_T	0.085	0.127	0.053	0.165
		B_T	54.937	50.982	55.874	51.873

functional groups such as -OH and -COOH, is the primary mechanism. This is further supported by the high R^2 values, indicating the availability of abundant uniform active sites on these adsorbents (Mahar et al., 2024).

The Freundlich isotherm, which assumes a heterogeneous adsorbent surface with multilayer adsorption, showed a better fit for HC with an R^2 of 0.985, compared to 0.917 for Areca husk and 0.731 for nano-HC. The Freundlich constant (n), which indicates adsorption favorability, was highest for Areca husk (2.831), suggesting favorable adsorption, while HC and nano-HC had lower values of 1.592 and 1.161, respectively. The KF values further supported this trend, with Areca husk demonstrating the highest value (24.272), followed by HC (8.685) and nano-HC (2.479). These results indicate that while nano-HC has the highest adsorption capacity, its adsorption process

is less influenced by the heterogeneity of the adsorbent surface compared to HC and Areca husk. This suggests that HC may involve contributions from multilayer adsorption and surface heterogeneity, as indicated by the relatively higher fit of the Freundlich model (Abebe et al., 2018).

The Temkin isotherm, which considers the effects of adsorbent-adsorbate interactions and the heat of adsorption, also provided insights into the adsorption process. For Areca husk, the Temkin model showed a good fit with an R^2 of 0.966, indicating significant adsorbent-adsorbate interactions. HC and nano-HC also demonstrated reasonable fits with R^2 values of 0.946 and 0.764, respectively. The K_T values, which represent the equilibrium binding constant, were highest for Areca husk (0.914), followed by HC (0.184) and nano-HC (0.085) (Wang and Guo, 2020b). The B_T values, related to the heat of adsorption, were

highest for nano-HC (54.937), suggesting stronger interactions at higher temperatures. These findings highlight the complex nature of the adsorption process, with different isotherms providing complementary insights. Overall, the results demonstrate the potential of nano-HC as a highly effective adsorbent for CR removal, particularly in scenarios requiring high adsorption capacity, while Areca husk and HC offer alternative pathways with moderate capacity and diverse adsorption mechanisms (Wang and Guo, 2020a).

According to the Table 4. Thermodynamic analysis of adsorption at different temperatures revealed distinct characteristics for the Areca husk, HC, and nano-HC adsorbents. The Areca husk exhibited a positive enthalpy change (ΔH) of 21.323 kJ/mol and a negative entropy change (ΔS) of -0.178 kJ/mol, indicating an endothermic process with decreasing randomness at the adsorbent-solution interface. The Gibbs free energy (ΔG) values were positive at all tested temperatures, including 51.902 kJ/mol at 303 K, 53.192 kJ/mol at 313 K, 54.236 kJ/mol at 323 K, and 55.121 kJ/mol at 333 K, suggesting that the adsorption process for Areca husk is non-spontaneous under these conditions.

For HC, the enthalpy change (ΔH) was 10.626 kJ/mol, and the entropy change (ΔS) was more negative at -0.615 kJ/mol. This indicates a less endothermic process with a significant decrease in system randomness. The Gibbs free energy (ΔG) values were also positive, increasing from 60.414 kJ/mol at 303 K to 65.282 kJ/mol at 333 K, confirming the non-spontaneity of the adsorption process for HC across the tested temperatures.

In contrast, nano-HC demonstrated a ΔH value of 15.174 kJ/mol, which is indicative of a moderately endothermic process. The entropy change (ΔS) was slightly negative at -0.155 kJ/mol, suggesting minimal reduction in entropy during adsorption. Similar to the other adsorbents, the Gibbs free energy (ΔG) values were positive, ranging from 62.856 kJ/mol at 303 K to 65.976 kJ/mol at 333 K, confirming the non-spontaneity of the process (Gamboa et al., 2024).

These results highlight that the adsorption processes for all three adsorbents – Areca husk, HC, and nano-HC – are endothermic in nature but non-spontaneous across the tested temperature range. The positive ΔH values indicate the necessity of energy input for the adsorption to occur, while the negative ΔS values reflect an overall

Table 4. Thermodynamic adsorption

Adsorbent	ΔH (kJ/mol)	ΔS (kJ/mol)	ΔG (kJ/mol)			
			303 K	313 K	323 K	333 K
Areca husk	21.323	-0.178	51.902	53.192	54.236	55.121
HC	10.626	-0.615	60.414	61.128	63.652	65.282
Nano HC	15.174	-0.155	62.856	62.914	64.473	65.976

Table 5. The adsorption capacity of another hydrochar source

Hydrochar source	Adsorbat	Qmax (Mg/G)	Literature
Bamboo sawdust	2-Naphthol	12.2	(Li et al., 2016)
Golden shower pod	Methylene Green	15.9	(Tran et al., 2017)
Coconut shell	Methylene Green	59.6	(Tran et al., 2017)
Orange peel	Methylene Green	32.7	(Tran et al., 2017)
Sunflower stalks	Methylene Blue	24.24	(Saini et al., 2024)
Longan peel	Malachite Green	117.647	(Wijaya et al., 2024)
Longan peel	Rhodamine B	50.505	(Wijaya et al., 2024)
Bamboo sawdust	Congo Red	33.7	(Li et al., 2018)
Garden waste	Methylene Blue	52.39	(Wu et al., 2024)
Rice straw	Congo Red	222.1	(Li et al., 2019)
Pomelo peel	Congo Red	144.9	(Zheng et al., 2020)
Areca husk	Congo Red	286.413	This study
Nano-hydrochar from areca husk	Congo Red	596.613	This study

reduction in disorder within the system during the process. The increasing ΔG values with temperature further underline the non-spontaneous nature of the adsorption under the examined conditions (Cabral et al., 2025) (Table 5).

Figure 8 shows that the adsorption mechanism can be further elucidated by analyzing the infrared (IR) spectroscopy data after adsorption. Post-adsorption IR spectra reveal significant changes indicating interactions between hydrochar or nano-hydrochar and dye molecules. The broad absorption band at $3400\text{--}3200\text{ cm}^{-1}$, associated with O–H stretching vibrations, shows shifts or intensity changes, suggesting hydrogen bonding or electrostatic interactions between hydroxyl groups on the adsorbent and the dye. Peaks around $1650\text{--}1600\text{ cm}^{-1}$, representing C=C stretching in aromatic rings, also exhibit intensity or position

changes, indicating $\pi\text{-}\pi$ interactions between the adsorbent’s aromatic structures and the dye molecules (Adawiyah et al., 2024). The peak at 1110 cm^{-1} , corresponding to C–O–C stretching in ether linkages, shows reduced intensity or shifts, implying that ether groups in carbohydrate residues participate in adsorption, likely through hydrogen bonding. The band at 1400 cm^{-1} , associated with C–H bending vibrations, also undergoes modifications, suggesting interactions between aliphatic chains and the dye. Additionally, new peaks or shifts in the IR spectrum after adsorption, such as those in the $1500\text{--}1300\text{ cm}^{-1}$ range, provide evidence of dye-adsorbent complex formation, indicating functional group interactions (Mahar et al., 2024).

These findings highlight that Congo red adsorption by HC and nano-HC involves a

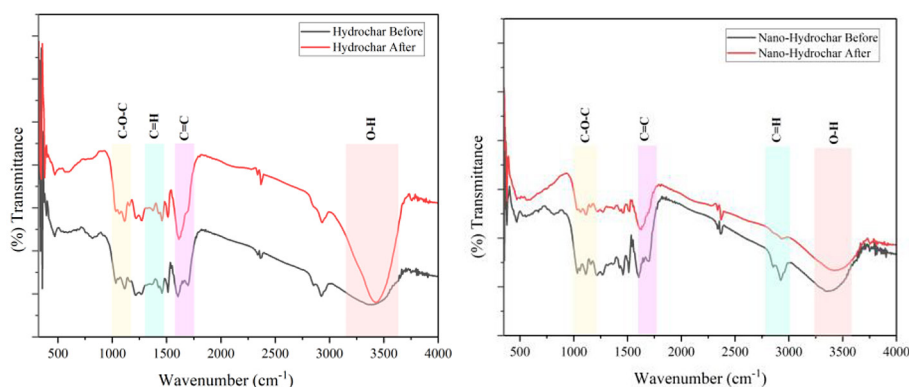


Figure 8. FTIR Spectrum of hydrochar and nano-hydrochar before and after adsorption

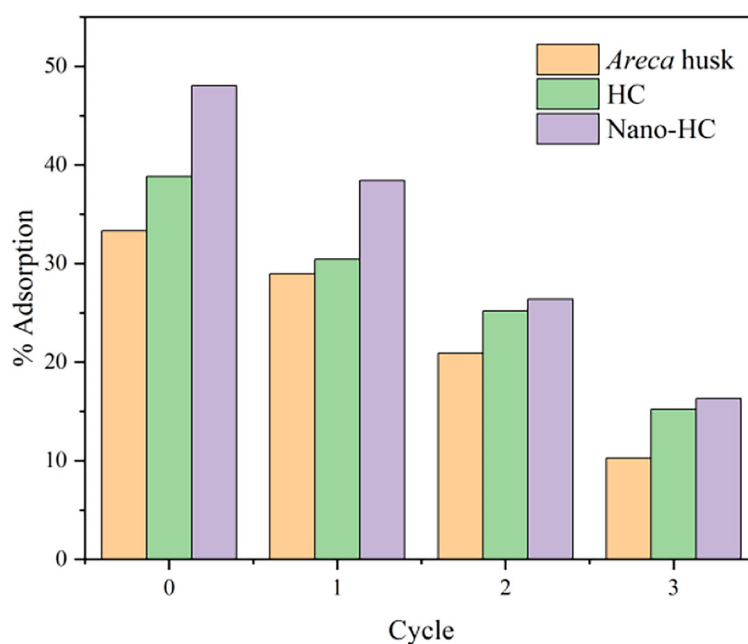


Figure 9. Regeneration cycle

combination of hydrogen bonding, π - π interactions, and electrostatic forces, enhancing adsorption efficiency. The IR data before and after adsorption offer detailed insights into the adsorption mechanism, supporting the potential of nano-HC as an effective adsorbent for dye-contaminated wastewater treatment (Sartape et al., 2017).

The regeneration process over three cycles showed that hydrochar and biochar retained their structural integrity, highlighting their potential as reusable adsorbents for CR removal. Figure 9 illustrates the regeneration of adsorbents: Areca fruit peel (a), hydrochar (b), and nano-hydrochar (c). Figure 5 shows that hydrochar and nano-hydrochar exhibit more stable regeneration and higher adsorption capacities compared to raw Areca fruit peel. The re-adsorption rates for HC and nano-HC, ranged from 56% to 15% over multiple cycles. In comparison, the re-adsorption capacity of raw Areca fruit peel after three cycles reached values in the range of 28.98% to 13.27%. Although the raw Areca fruit peel had a lower initial adsorption capacity, it showed comparable re-adsorption capacities after several cycles, particularly after the third cycle.

However, both HC and nano-HC experienced a decline in adsorption capacity and structural stability across cycles, likely due to the degradation of organic components during repeated adsorption-desorption processes (Mumme et al., 2011). These findings suggest that converting Areca fruit peel into HC or nano-HC improves the structural stability and reusability of the adsorbent, making them more robust materials for Congo red removal in practical applications. Specifically, nano-HC demonstrated the highest initial adsorption capacity (48.04%) with a decline to 15.30% after four cycles, showing its potential for multiple reuses (Srivatsav et al., 2020).

CONCLUSIONS

This study demonstrates that the hydrothermal carbonization process combined with high-energy milling significantly enhances the structural and adsorption properties of Areca husk. A comparative analysis revealed that nano-hydrochar exhibits superior characteristics compared to HC and raw Areca husk, including higher surface area, porosity, and oxygen-containing functional groups. Adsorption capacities for Congo red were 596.617 mg/g for nano-HC, 356.132 mg/g for

HC, and 128.654 mg/g for raw Areca husk, showing a significant enhancement with nanostructuring. Adsorption kinetics for all materials followed the pseudo-second-order (PSO) model, indicating chemisorption, while the Langmuir isotherm suggested monolayer adsorption. Regeneration studies highlighted the superior stability and reusability of nano-HC, underscoring its potential as an advanced, sustainable adsorbent for dye removal in wastewater treatment.

Acknowledgement

The authors would like to express their gratitude to the Research Center for Inorganic Materials and Complexes, FMIPA Universitas Sriwijaya, for their support in providing laboratory analysis. This research also the additional output from SATEKS Unsri grant, number 0012/UN9/SK.LP2M.PT/2024. Additionally, the authors would like to thank the National Research and Innovation Agency (BRIN) for assisting in the pyrolysis process and material characterization.

REFERENCES

1. Abebe, B., Murthy, H. C. A., & Amare, E. (2018). Summary on Adsorption and Photocatalysis for Pollutant Remediation: Mini Review. *Journal of Encapsulation and Adsorption Sciences*, 8(4), 225–255. <https://doi.org/10.4236/jeas.2018.84012>
2. Adawiyah, R., Yuliasari, N., Hanifah, Y., Alawiyah, K., & Rahayu Palapa, N. (2024). Utilizing *Areca catechu* L. Fruit Peel-Derived Biochar and Hydrochar for Congo Red Adsorption: Kinetic and Thermodynamic Analysis. *Indonesian Journal of Environmental Management and Sustainability*, 8(4), 135–144. <https://doi.org/10.26554/ijems.2024.8.4.135-144>
3. Bardalai, M., & Mahanta, D. K. (2018). Characterisation of Biochar Produced by Pyrolysis from Areca Catechu Dust. In *Materials Today: Proceedings 5*. www.sciencedirect.com/www.materialstoday.com/proceedings2214-7853
4. Bo, J., & Shi, B. (2024). Performances of residues from hydrolyzed corn-cobs for the adsorption of Congo red. *Industrial Crops and Products*, 220, 119311. <https://doi.org/10.1016/j.indcrop.2024.119311>
5. Cabral, L. L., Bottini, R. C. R., Gonçalves, A. J., Junior, M. M., Rizzo-Domingues, R. C. P., Lenzi, M. K., Nagalli, A., Passig, F. H., dos Santos, P. M., & de Carvalho, K. Q. (2025). Food dye adsorption in single and ternary systems by the novel passion fruit peel biochar adsorbent. *Food*

- Chemistry*, 464, 141592. <https://doi.org/10.1016/j.foodchem.2024.141592>
6. Chao, F.-L., Yang, T.-H., & Wu, J.-Y. (2020). New uses for Areca Catechu tree. *International Wood Products Journal*, 11(2), 94–100. <https://doi.org/10.1080/20426445.2020.1732525>
 7. Chausali, N., Saxena, J., & Prasad, R. (2021). Nanobiochar and biochar based nanocomposites: Advances and applications. *Journal of Agriculture and Food Research*, 5, 100191. <https://doi.org/10.1016/j.jafr.2021.100191>
 8. Dai, Y., Zhang, N., Xing, C., Cui, Q., & Sun, Q. (2019). The adsorption, regeneration and engineering applications of biochar for removal organic pollutants: A review. *Chemosphere*, 223, 12–27. <https://doi.org/10.1016/j.chemosphere.2019.01.161>
 9. Emmanuel, S. S., & Adesibikan, A. A. (2024a). Hydrothermal valorization of biomass waste into hydrochar towards circular economy and sustainable adsorptive dye contaminants clean-up: A review. *Desalination and Water Treatment*, 320, 100801. <https://doi.org/10.1016/j.dwt.2024.100801>
 10. Emmanuel, S. S., & Adesibikan, A. A. (2024b). Hydrothermal valorization of biomass waste into hydrochar towards circular economy and sustainable adsorptive dye contaminants clean-up: A review. *Desalination and Water Treatment*, 320, 100801. <https://doi.org/10.1016/j.dwt.2024.100801>
 11. Gamboa, D. M. P., Abatal, M., Lima, E., Franseschi, F. A., Uacán, C. A., Tariq, R., Elías, M. A. R., & Vargas, J. (2024). Sorption Behavior of Azo Dye Congo Red onto Activated Biochar from Haematoxylum campechianum Waste: Gradient Boosting Machine Learning-Assisted Bayesian Optimization for Improved Adsorption Process. *International Journal of Molecular Sciences*, 25(9), 4771. <https://doi.org/10.3390/ijms25094771>
 12. Gao, P., Zhou, Y., Meng, F., Zhang, Y., Liu, Z., Zhang, W., & Xue, G. (2016). Preparation and characterization of hydrochar from waste eucalyptus bark by hydrothermal carbonization. *Energy*, 97, 238–245. <https://doi.org/10.1016/j.energy.2015.12.123>
 13. Goyi, A. A., Sher Mohammad, N. M., & Omer, K. M. (2024). Preparation and characterization of potato peel derived hydrochar and its application for removal of Congo red: a comparative study with potato peel powder. *International Journal of Environmental Science and Technology*, 21(1), 631–642. <https://doi.org/10.1007/s13762-023-04965-y>
 14. Guo, S., Dong, X., Wu, T., Shi, F., & Zhu, C. (2015). Characteristic evolution of hydrochar from hydrothermal carbonization of corn stalk. *Journal of Analytical and Applied Pyrolysis*, 116, 1–9. <https://doi.org/10.1016/j.jaap.2015.10.015>
 15. Hammud, H. H., Hammoud, M. H., Hussein, A. A., Fawaz, Y. B., Abdul Hamid, M. H. S., & Sheikh, N. S. (2023). Removal of Malachite Green Using Hydrochar from PALM Leaves. *Sustainability*, 15(11), 8939. <https://doi.org/10.3390/su15118939>
 16. Haris, M., Khan, M. W., Paz-Ferreiro, J., Mahmood, N., & Eshtiaghi, N. (2022). Synthesis of functional hydrochar from olive waste for simultaneous removal of azo and non-azo dyes from water. *Chemical Engineering Journal Advances*, 9, 100233. <https://doi.org/10.1016/j.ceja.2021.100233>
 17. Harja, M., Buema, G., & Bucur, D. (2022). Recent advances in removal of Congo Red dye by adsorption using an industrial waste. *Scientific Reports*, 12(1), 6087. <https://doi.org/10.1038/s41598-022-10093-3>
 18. Hasanah, M., Wijaya, A., Arsyad, F. S., Mohadi, R., & Lesbani, A. (2022). Preparation of Hydrochar from Salacca zalacca Peels by Hydrothermal Carbonization: Study of Adsorption on Congo Red Dyes and Regeneration Ability. *Science and Technology Indonesia*, 7(3), 372–378. <https://doi.org/10.26554/sti.2022.7.3.372-378>
 19. Hua, Z., Pan, Y., & Hong, Q. (2023). Adsorption of Congo red dye in water by orange peel biochar modified with CTAB. *RSC Advances*, 13(18), 12502–12508. <https://doi.org/10.1039/D3RA01444D>
 20. Jalilian, M., Bissessur, R., Ahmed, M., Hsiao, A., He, Q. S., & Hu, Y. (2024a). A review: Hydrochar as potential adsorbents for wastewater treatment and CO₂ adsorption. *Science of The Total Environment*, 914, 169823. <https://doi.org/10.1016/j.scitotenv.2023.169823>
 21. Jalilian, M., Bissessur, R., Ahmed, M., Hsiao, A., He, Q. S., & Hu, Y. (2024b). A review: Hydrochar as potential adsorbents for wastewater treatment and CO₂ adsorption. *Science of The Total Environment*, 914, 169823. <https://doi.org/10.1016/j.scitotenv.2023.169823>
 22. Khan, A. A., Naqvi, S. R., Ali, I., Farooq, W., Anjum, M. W., AlMohamadi, H., Lam, S. S., Verma, M., Ng, H. S., & Liew, R. K. (2023). Algal biochar: A natural solution for the removal of Congo red dye from textile wastewater. *Journal of the Taiwan Institute of Chemical Engineers*, 105312. <https://doi.org/10.1016/j.jtice.2023.105312>
 23. Kumar, A., Saini, K., & Bhaskar, T. (2020). Hydrochar and biochar: Production, physicochemical properties and techno-economic analysis. In *Bioresource Technology* 310. <https://doi.org/10.1016/j.biortech.2020.123442>
 24. Lin, Z., Wang, R., Tan, S., Zhang, K., Yin, Q., Zhao, Z., & Gao, P. (2023). Nitrogen-doped hydrochar prepared by biomass and nitrogen-containing wastewater for dye adsorption: Effect of nitrogen source in wastewater on the adsorption performance of hydrochar. *Journal of Environmental Management*, 334, 117503. <https://doi.org/10.1016/j.jenvman.2023.117503>

25. Liu, C., Balasubramanian, P., Li, F., & Huang, H. (2024). Machine learning prediction of dye adsorption by hydrochar: Parameter optimization and experimental validation. *Journal of Hazardous Materials*, *480*, 135853. <https://doi.org/10.1016/j.jhazmat.2024.135853>
26. Li, Y., Meas, A., Shan, S., Yang, R., & Gai, X. (2016). Production and optimization of bamboo hydrochars for adsorption of Congo red and 2-naphthol. *Bioresource Technology*, *207*, 379–386. <https://doi.org/10.1016/j.biortech.2016.02.012>
27. Li, Y., Meas, A., Shan, S., Yang, R., Gai, X., Wang, H., & Tsend, N. (2018). Characterization, isotherm and kinetic data for adsorption of Congo red and 2-naphthol on different bamboo hydrochars. *Data in Brief*, *19*, 49–54. <https://doi.org/10.1016/j.dib.2018.04.066>
28. Li, Y., Tsend, N., Li, T., Liu, H., Yang, R., Gai, X., Wang, H., & Shan, S. (2019). Microwave assisted hydrothermal preparation of rice straw hydrochars for adsorption of organics and heavy metals. *Bioresource Technology*, *273*, 136–143. <https://doi.org/10.1016/j.biortech.2018.10.056>
29. Mahar, D., Semwal, N., Aneja, A., & Arya, M. C. (2024). Rapid adsorptive removal of congo red using Cu/Fe/Al mixed metal oxides obtained from layered double hydroxide nanomaterial: Performance and optimization evaluation using BBD-RSM approach. *Surfaces and Interfaces*, *55*, 105366. <https://doi.org/10.1016/j.surfin.2024.105366>
30. Mahmoud, A. E. D., Ali, R., & Fawzy, M. (2024). Insights into levofloxacin adsorption with machine learning models using nano-composite hydrochars. *Chemosphere*, *355*, 141746. <https://doi.org/10.1016/j.chemosphere.2024.141746>
31. Mumme, J., Eckervogt, L., Pielert, J., Diakité, M., Rupp, F., & Kern, J. (2011). Hydrothermal carbonization of anaerobically digested maize silage. *Bioresource Technology*, *102*(19), 9255–9260. <https://doi.org/10.1016/j.biortech.2011.06.099>
32. Normah, N., Juleanti, N., Siregar, P. M. S. B. N., Wijaya, A., Palapa, N. R., Taher, T., & Lesbani, A. (2021). Size Selectivity of Anionic and Cationic Dyes Using LDH Modified Adsorbent with Low-Cost Rambutan Peel to Hydrochar. *Bulletin of Chemical Reaction Engineering & Catalysis*, *16*(4), 869–880. <https://doi.org/10.9767/brec.16.4.12093.869-880>
33. Palapa, N. R., Taher, T., Wijaya, A., & Lesbani, A. (2021). Modification of Cu/Cr Layered Double Hydroxide by Keggin Type Polyoxometalate as Adsorbent of Malachite Green from Aqueous Solution. *Science and Technology Indonesia*, *6*(3), 209–217. <https://doi.org/10.26554/sti.2021.6.3.209-217>
34. Pauletto, P. S., Moreno-Pérez, J., Hernández-Hernández, L. E., Bonilla-Petriciolet, A., Dotto, G. L., & Salau, N. P. G. (2021). Novel biochar and hydrochar for the adsorption of 2-nitrophenol from aqueous solutions: An approach using the PVSDM model. *Chemosphere*, *269*, 128748. <https://doi.org/10.1016/j.chemosphere.2020.128748>
35. Ren, X., Chen, C., Nagatsu, M., & Wang, X. (2011). Carbon nanotubes as adsorbents in environmental pollution management: A review. *Chemical Engineering Journal*, *170*(2–3), 395–410. <https://doi.org/10.1016/j.cej.2010.08.045>
36. Rojas-Chávez, H., Juárez-García, J. M., Herrera-Rivera, R., Flores-Rojas, E., González-Domínguez, J. L., Cruz-Orea, A., Cayetano-Castro, N., Ávila-García, A., & Mondragón-Sánchez, M. L. (2020). The high-energy milling process as a synergistic approach to minimize the thermal conductivity of PbTe nanostructures. *Journal of Alloys and Compounds*, *820*, 153167. <https://doi.org/10.1016/j.jallcom.2019.153167>
37. Saini, R., Pandey, M., Mishra, R. K., & Kumar, P. (2024). Adsorption potential of hydrochar derived from hydrothermal carbonization of waste biomass towards the removal of methylene blue dye from wastewater. *Biomass Conversion and Biorefinery*. <https://doi.org/10.1007/s13399-024-05743-7>
38. Sartape, A. S., Mandhare, A. M., Jadhav, V. V., Raut, P. D., Anuse, M. A., & Kolekar, S. S. (2017). Removal of malachite green dye from aqueous solution with adsorption technique using Limonia acidissima (wood apple) shell as low cost adsorbent. *Arabian Journal of Chemistry*, *10*, S3229–S3238. <https://doi.org/10.1016/j.arabjc.2013.12.019>
39. Sharma, P. K., Kumar, R., Singh, R. K., Sharma, P., & Ghosh, A. (2022). Review on arsenic removal using biochar-based materials. *Groundwater for Sustainable Development*, *17*, 100740. <https://doi.org/10.1016/j.gsd.2022.100740>
40. Singh, D. K., & Garg, A. (2024). Application of sewage sludge derived hydrochar as an adsorbent for removal of methylene blue. *Sustainable Chemistry for the Environment*, *8*, 100158. <https://doi.org/10.1016/j.scenv.2024.100158>
41. Siregar, P. M. S. B. N., Palapa, N. R., Wijaya, A., Fitri, E. S., & Lesbani, A. (2021). Structural Stability of Ni/Al Layered Double Hydroxide Supported on Graphite and Biochar Toward Adsorption of Congo Red. *Science and Technology Indonesia*, *6*(2), 85–95. <https://doi.org/10.26554/sti.2021.6.2.85-95>
42. Srivatsav, P., Bhargav, B. S., Shanmugasundaram, V., Arun, J., Gopinath, K. P., & Bhatnagar, A. (2020). Biochar as an Eco-Friendly and Economical Adsorbent for the Removal of Colorants (Dyes) from Aqueous Environment: A Review. *Water*, *12*(12), 3561. <https://doi.org/10.3390/w12123561>
43. Supraja, K. V., Doddapaneni, T. R. K. C., Ramasamy, P. K., Kaushal, P., Ahammad, Sk. Z., Pollmann, K., & Jain, R. (2023). Critical review on production,

- characterization and applications of microalgal hydrochar: Insights on circular bioeconomy through hydrothermal carbonization. *Chemical Engineering Journal*, 473, 145059. <https://doi.org/10.1016/j.cej.2023.145059>
44. Tabassum, M., Bardhan, M., Novera, T. M., Islam, Md. A., Hadi Jawad, A., & Islam, Md. A. (2020). NaOH-Activated Betel Nut Husk Hydrochar for Efficient Adsorption of Methylene Blue Dye. *Water, Air, & Soil Pollution*, 231(8), 398. <https://doi.org/10.1007/s11270-020-04762-0>
45. Tran, H. N., You, S.-J., & Chao, H.-P. (2017). Insight into adsorption mechanism of cationic dye onto agricultural residues-derived hydrochars: Negligible role of π - π interaction. *Korean Journal of Chemical Engineering*, 34(6), 1708–1720. <https://doi.org/10.1007/s11814-017-0056-7>
46. Vinayagam, R., Kandati, S., Murugesan, G., Govindas, L. C., Baliga, A., Pai, S., Varadavenkatesan, T., Kaviyarasu, K., & Selvaraj, R. (2023). Bioinspiration synthesis of hydroxyapatite nanoparticles using eggshells as a calcium source: Evaluation of Congo red dye adsorption potential. *Journal of Materials Research and Technology*, 22, 169–180. <https://doi.org/10.1016/j.jmrt.2022.11.093>
47. Waly, S. M., El-Wakil, A. M., Abou El-Maaty, W. M., & Awad, F. S. (2024). Hydrothermal synthesis of Mg/Al-layered double hydroxide modified water hyacinth hydrochar for remediation of wastewater containing mordant brown dye. *RSC Advances*, 14(22), 15281–15292. <https://doi.org/10.1039/D4RA02624A>
48. Wang, D., Liu, L., Jiang, X., Yu, J., & Chen, X. (2015). Adsorption and removal of malachite green from aqueous solution using magnetic β -cyclodextrin-graphene oxide nanocomposites as adsorbents. *Colloids and Surfaces A: Physicochemical and Engineering Aspects*, 466, 166–173. <https://doi.org/10.1016/j.colsurfa.2014.11.021>
49. Wang, J., & Guo, X. (2020a). Adsorption isotherm models: Classification, physical meaning, application and solving method. *Chemosphere*, 258, 127279. <https://doi.org/10.1016/j.chemosphere.2020.127279>
50. Wang, J., & Guo, X. (2020b). Adsorption kinetic models: Physical meanings, applications, and solving methods. *Journal of Hazardous Materials*, 390, 122156. <https://doi.org/10.1016/j.jhazmat.2020.122156>
51. Wang, Z., Tang, Z., Xie, X., Xi, M., & Zhao, J. (2022). Salt template synthesis of hierarchical porous carbon adsorbents for Congo red removal. *Colloids and Surfaces A: Physicochemical and Engineering Aspects*, 648, 129278. <https://doi.org/10.1016/j.colsurfa.2022.129278>
52. Wijaya, A., Ardiansyah, R., Augustiara, E., & Fajri, S. (2024). Preparation of Hydrochar from Longan Peel: A Promising Adsorbent for Cationic Dye Removal in Aqueous Solutions. *Indonesian Journal of Material Research*, 2(3), 79–85. <https://doi.org/10.26554/ijmr.20242344>
53. Wijaya, A., Siregar, P. M. S. B. N., Priambodo, A., Palapa, N. R., Taher, T., & Lesbani, A. (2021). Innovative Modified of Cu-Al/C (C = Biochar, Graphite) Composites for Removal of Procion Red from Aqueous Solution. *Science and Technology Indonesia*, 6(4). <https://doi.org/10.26554/sti.2021.6.4.228-234>
54. Wu, C., Zhao, Z., Zhong, J., Lv, Y., Yan, X., Wu, Y., & Zhang, H. (2024). Adsorption of dye through hydrochar derived from co-hydrothermal carbonization of garden waste and sewage sludge: The adsorption enhancement mechanism of lignin component. *Journal of Water Process Engineering*, 67, 106233. <https://doi.org/10.1016/j.jwpe.2024.106233>
55. Zahara, Z. A., Royani, I., Palapa, N. R., Mohadi, R., & Lesbani, A. (2023). Treatment of Methylene Blue Using Ni-Al/Magnetite Biochar Layered Double Hydroxides Composite by Adsorption. *Bulletin of Chemical Reaction Engineering & Catalysis*, 18(4), 659–674. <https://doi.org/10.9767/brec.20049>
56. Zhang, D. L., Liu, Z. G., & Koch, C. C. (2004). Applications of High Energy Mechanical Milling in Processing Advanced Materials: An Overview of the Understanding. *Journal of Metastable and Nanocrystalline Materials*, 20–21, 103–110. <https://doi.org/10.4028/www.scientific.net/JMNM.20-21.103>
57. Zheng, H., Sun, Q., Li, Y., & Du, Q. (2020). Biosorbents prepared from pomelo peel by hydrothermal technique and its adsorption properties for congo red. *Materials Research Express*, 7(4), 045505. <https://doi.org/10.1088/2053-1591/ab8a83>
58. Zhou, B., Wang, J. J., Dangal, P., Lomnicki, S., Roy, A. D., & Park, J.-H. (2024). A novel sugarcane residue-derived bimetallic Fe/Mn-biochar composite for activation of peroxymonosulfate in advanced oxidation process removal of azo dye: Degradation behavior and mechanism. *Journal of Water Process Engineering*, 58, 104740. <https://doi.org/10.1016/j.jwpe.2023.104740>